Microfluidic analog of the four-roll mill

S. D. Hudson,[a] F. R. Phelan, Jr., M. D. Handler, J. T. Cabral, K. B. Migler, and E. J. Amis
Polymers Division, National Institute of Standards and Technology, Gaithersburg, Maryland 20899-8544

(Received 12 March 2004; accepted 7 May 2004)

We describe a *microfluidic trap*, for analysis of fluids and suspensions, that simulates the function of a four-roll mill, a rheological tool with adjustable flow type and rate. These flow characteristics were designed with the assistance of flow simulations and are measured here by micro-particle-image-velocimetry. This miniature device permits microscopic manipulations and measurements (e.g., of cells, particles, and drops) and it is capable of a range of flow types, including simple shear. [DOI: 10.1063/1.1767594]

When assembling advanced materials, the type and strength of flow are often crucial to produce the desired structure and properties. For example, high strength fibers are drawn in highly extensional flow to create substantial molecular alignment.[1] In contrast, simple shear flow is inefficient for molecular alignment, but is frequently encountered during materials processing. For electro-optic and other advanced materials, flow and electric fields may be used together to establish the necessary structure.[2]

Whereas material may transit quickly through a production process, devices with stagnation points facilitate measurement of the kinetic and steady material responses. The four-roll mill, pioneered by Taylor,[3] is ideal for this purpose, because it provides adjustable flow type and rate, at the stagnation point, by regulating the speed and direction of the four rollers.[4,5] Such tools have been used to measure flow-induced molecular alignment,[6] crystallization,[7] and drop deformation,[3,8,9] breakup[3,8] and coalescence.[10] We now seek to develop an analogous device, using recent advances of microfluidic technology[11–13] which suggest that fine flow control can be exploited for micro- and nanoassembly and characterization of materials. For example, microfluidic tools and high-resolution optics recently permitted the direct observation of the molecular response to flow.[14,15] These devices, however, have only a single fixed flow type.

Generally, fluid flow may comprise different amounts of stretching and rotation. For example, rotation is absent in extensional flow, whereas in simple shear flow the rate of rotation and stretching are equal. Any mixture of rotation and extension is possible. We classify flow fields in terms of a (frame invariant) flow type ξ and shear rate G, based on Astarita's criterion.[16] In this context, for extensional, simple shear and rotational flow, ξ equals 1, 0, and −1, respectively.

To design a suitable microfluidic four-roll mill equivalent, the means to control stretching and rotation at a stagnation point are required. First, pure stretching is produced at opposing jets, such as when channels are arranged as the four arms of a cross. For example, if fluid enters from the top and bottom arms and leaves to the left and right, a stagnation point occurs at the center, where the flow is extensional. Although viscous flow within each of the arms is non-linear, flow is linear near the stagnation point. Second, rotation is introduced, if the opposing arms are offset, or within a cavity adjacent to the stream.[17] These two principles have been combined in a cross channel design, comprising six channels, with dividers between channels in a chiral arrangement (Fig 1).

Three-dimensional Stokes flow simulations demonstrate that the ratio of channel height to width h/w must be greater than unity to produce substantial rotation (Fig. 2; for additional results see EPAPS Ref. 18). When h/w is small, the flow type is nearly always purely extensional at the stagnation point. Large h/w is also beneficial for flow uniformity. For these reasons, a device with $h/w \approx 2.8$ was fabricated (Fig 1).

Micro-particle-image-velocimetry (μPIV) was used to map the flow field in the device as a function of the relative flow rates in the microchannels. The flow rate in channels 3 and 4 were set equal to that of channels 1 and 2, respectively (i.e., $Q_1 = Q_3; Q_2 = Q_4$; Fig. 1). The ratio Q_1/Q_2 was adjusted between −0.2 and 1.7, where negative values of Q_1 signify withdrawal of fluid away from the intersection. Figure 3 shows a sample image obtained in a flow condition that approximates extensional flow at the stagnation ($Q_1/Q_2 \approx 0.8$). Velocity vectors determined by cross correlation of sequential images are shown overlaid on the image (videos in EPAPS Ref. 18).

Characteristics G and ξ of the velocity vector field within a radius of several interrogation points near the stagnation point were determined (Fig. 4) by a best fit to a linear flow field, with velocity components $u = \mathrm{G}y$ and $v = G\xi x$, where an appropriate coordinate transformation is made (see methods). The vorticity is given by: $\omega = 1/2G(1-\xi)$. By adjusting flow rate ratios, the flow type ranges from approxi-

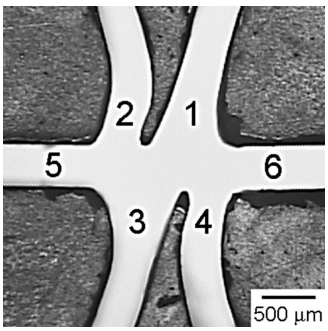

FIG. 1. Reflected light micrograph of the device master, engraved in wax (1100 μm thick slab). The open channels (400 μm wide; $h/w \approx 2.8$) appear white and are labeled numerically. The dividers between flow channels 1 and 2 (and 3 and 4) are ~120 μm wide (aspect ratio ≈ 9).

[a]Electronic mail: steven.hudson@nist.gov

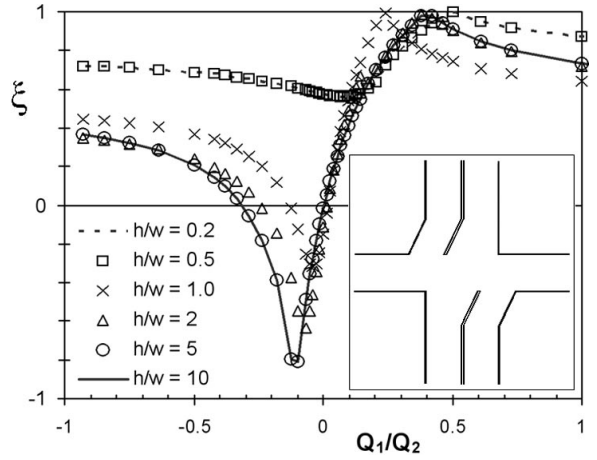

FIG. 2. Flow type ξ computed as a function of the ratio of flow rates in channels Q_1/Q_2, for Stokes flow in three dimensions. The plan-view channel simulation geometry is inset at lower right (cf. Fig. 1). The minimum flow type depends significantly on the aspect ratio h/w. When h/w is small, the flow at the stagnation point is nearly extensional for all values of Q_1/Q_2. Asymptotic behavior is observed: note the essential agreement of results at $h/w=0.2$ and 0.5, and at 5 and 10.

mately −0.37 to 0.83. In actuality, since the vorticity varies continuously through zero,[18] pure extensional flow (i.e., $\xi=1.0$) will be obtained when the vorticity vanishes, which occurs when the flow rate ratio $Q_1/Q_2 \approx 0.7$, in this device. Rotation is counterclockwise at smaller values of this ratio, and clockwise at larger values. The experimental results (Fig. 4) are qualitatively consistent with the simulation of a similar geometry (Fig. 2). Quantitative agreement is expected if the geometries match exactly. This device produces a wide range of flow types, ranging from highly rotational to extensional. Both simulations and experiments demonstrate that even simple shear (i.e., $\xi=0$) is attainable (Figs. 2 and 4, and EPAPS Ref. 18). In contrast, $|\xi|<0.2$ is inaccessible in the four-roll mill.[10,19] Although these experiments and simulations apply to viscous fluids, a range of flow types would also be possible when inertial or elastic effects are significant. Recently, elasticity was used to create bistable shear flow patterns in microfluidic devices.[20]

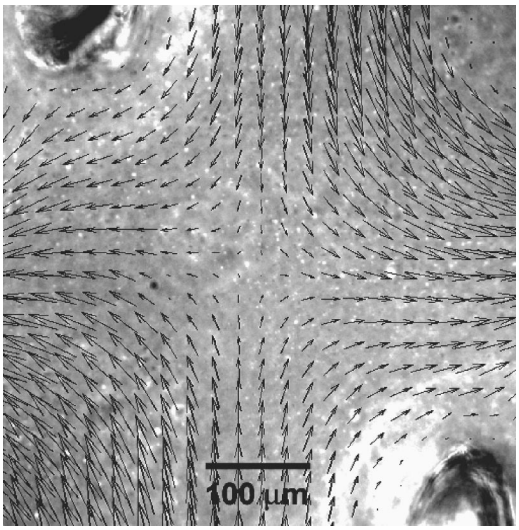

FIG. 3. Phase contrast optical micrograph and μPIV vector overlay when $Q_1=4$ μL/min and $Q_2=5$ μL/min. Additional data and videos are available in EPAPS Ref. 18.

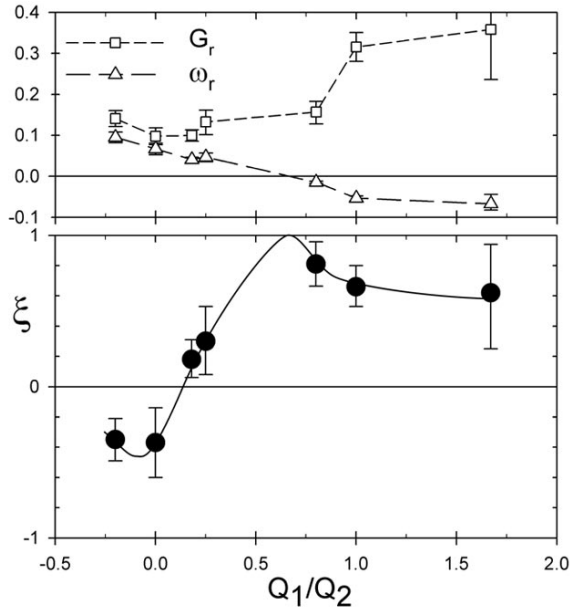

FIG. 4. Flow type ξ, relative flow magnitude G_r, and the relative vorticity ω_r as a function of dependence on Q_1/Q_2. Standard uncertainties (associated with a fit to μPIV data) are indicated by the error bars. For flow type, a curve qualitatively similar to Fig. 2 is drawn to guide the eye. $G_r=|G/G_o|$, where G_o is the rms value of the average G in the input and output channels, and $\omega_r=\omega/|\omega_o|$ where $\omega_o=G_o/2$. These results indicate that flow of type $\xi>0$ are relatively efficient, in comparison to predominantly rotational flows.

After achieving tunable and wide flow types, we now seek to explore transient flows. The ability to adjust flow conditions quickly is essential for two reasons. First, the flow must be able to be switched on and off faster than the material response time, to study transient behavior. Second, since material at the stagnation point is unstable to fluctuations in position (along the outflow axis), active adjustment of the location of the stagnation point, by changing the balance of flow rates in opposite flow channels, is desirable.[4] The maximum flow rate compatible with such active control (to maintain objects at the stagnation point) is limited by the device response time, which can be optimized by appropriate choice of tubing (considering hydrodynamic resistance and volumetric capacitance) and efficient coupling of syringes and pumps. This response time can be on the order of the video frame interval (e.g., 0.04 s), and we have been able to hold objects (such as liquid drops and red blood cells) in these microfluidic traps where G is in excess of 1 s^{-1} for several minutes; for experiments with red blood cells, positional fluctuations along the outflow axis are less than ± 2 μm.

Likewise, since vorticity is a continuous function of Q_1/Q_2 (confirmed by simulation), tuning this ratio permits rational control of the orientation of an object, and of the angle of collision (e.g., head-on) of a pair of drops or particles.

In conclusion, we demonstrate unprecedented flow control with a simple microfluidic tool: achieving the complete range of planar flow type, including simple shear, and actively trapping particles at the stagnation point. These accomplishments open new avenues for advanced materials assembly and interrogation in microfluidics.

The Navier-Stokes equation, subject to an incompressibility condition, was solved by finite element method (FIex-PDE, PDE Solutions, Inc.[21]):

$$\rho \underline{u} \cdot \nabla \underline{u} = -\nabla p + \eta \nabla^2 \underline{u},$$
$$\nabla^2 p = -\nabla \cdot \nabla \cdot (\rho \underline{u}\underline{u}) + \beta \nabla \cdot \underline{u}, \tag{1}$$

where ρ (=0, i.e., Stokes limit) is the fluid density, η (=1) is its viscosity, p $[O(1)]$ is pressure, and β is a large constant (=1000) that ensures that $\nabla \cdot \underline{u}$ is negligible. The flow type is defined:

$$\xi = \frac{\underline{\underline{D}}:\underline{\underline{D}} + \underline{\underline{W}}:\underline{\underline{W}}}{\underline{\underline{D}}:\underline{\underline{D}} - \underline{\underline{W}}:\underline{\underline{W}} + 2\sqrt{(\underline{\underline{D}}:\underline{\underline{D}})(-\underline{\underline{W}}:\underline{\underline{W}})}}, \tag{2}$$

in terms of the tensorial rates of stretching $\underline{\underline{D}}$ and rotation $\underline{\underline{W}}$ (relative to the material rotation of the principal axes of $\underline{\underline{D}}$). (Additional parameters would be required if the axis of rotation did not coincide with one of the principal axes of the stretching tensor.[19]) Note that the quantity $\underline{\underline{W}}:\underline{\underline{W}}$ is negative. Assuming incompressible flow (i.e., traceless tensors), we can rewrite this expression in terms of the principal eigenvalues of these tensors:

$$\xi = \frac{D_1^2 - W_1^2}{(D_1 + W_1)^2} = \frac{D_1 - W_1}{D_1 + W_1}. \tag{3}$$

Accordingly, the shear rate is: $G = D_1 + W_1$. At the stagnation point, these quantities are equivalent to the nonobjective parameters used by others.[10,14]

The geometry of the channels in x and y dimensions is sketched in the inset of Fig. 2. The width of the channels w is unity, and their length is 10, representative of the device. The flow field was computed for several values of the channel height h: 0.2, 0.5, 1, 2, 5, and 10.

To rapidly fabricate channels with sufficiently high aspect ratio, a master was carved from jewelers engraving wax (Fig. 1). Various micromachining and lithographic processes are feasible alternatives. This positive master was then replicated in two steps, using polydimethylsiloxane (PDMS) elastomer, to produce the microchannel device. Sylguard 184 silicone (Dow Corning) resin and curing agent were mixed, 10:1 by mass fraction, and cured at 75°C for 1 h. The first replication step produced a solid negative form, which was treated in an UV-ozone cleaner for 10 min and then at 75°C for several hours. This negative master was replicated again in like manner. The resulting PDMS device was treated briefly (1.5 min) with UV ozone before irreversibly bonding onto a clean glass substrate (treated in an UV-ozone cleaner for 1 h). Stainless steel connectors were inserted in the device through holes made using a sharpened tubular bore, and the entire assembly was heat treated for ~6 h to promote bonding of the PDMS and glass.

The "particles" for μPIV were emulsion drops of 2.0% mass fraction poly[dimethylsiloxane-b-(ethyleneglycol-co-propyleneglycol)] in poly(propyleneglycol); the viscosity of the latter at 25°C is 5.2 Pa s. The mixture forms a stable emulsion, and was prepared by magnetically stirring for ~3 h at 25°C. Velocimetry experiments were performed at $G \sim 1\ s^{-1}$, so that the drops remain nearly spherical in the flow. This emulsion was viewed by phase contrast microscopy (Olympus) using a 10× objective lens having a numerical aperture NA=0.30. Drops in proximity of the focal plane appear bright or dark, depending on whether they are closer or farther, respectively, from the objective lens. Particles outside the depth of field ($\approx \pm 10\ \mu$m) are indistinguishable from the uniform grey background. The focal plane was adjusted halfway between the upper and lower channel surfaces. Channels labeled 1–4 (Fig. 1) were connected to independent syringe pumps. Channels 5 and 6 (Fig. 1) were connected through a T connection to a common waste line. 1 M pixel images (Fig. 3) were recorded using an exposure time of 0.01 s and a frequency of 20 Hz. Cross correlation was computed of 64×64 pixel subunits of sequential images (with a low pass Gaussian filter applied). These super-pixel interrogation areas were overlapped by 50%. As noted above, these flow maps were fitted with a generalized linear flow field:

$$\begin{bmatrix} u \\ v \end{bmatrix} = G \begin{bmatrix} \cos\psi & -\sin\psi \\ \sin\psi & \cos\psi \end{bmatrix} \begin{bmatrix} -\sin\psi & \cos\psi \\ \xi\cos\psi & \xi\sin\psi \end{bmatrix} \begin{bmatrix} x - x_o \\ x - y_o \end{bmatrix}, \tag{4}$$

x_o, y_o are the coordinates of the stagnation point, $\psi + \pi/4$ is the orientation of the principal stretching axis with respect to the x axis.

Device control, image acquisition, and active feedback were accomplished using a LabVIEW Program that was developed for this purpose.

[1] D. C. Prevorsek, in *Handbook of Fiber Science and Technology, Vol. 3, Part D: High Technology Fibers*, edited by M. Lewin and J. Preston (Marcel Dekker, New York, 1996).
[2] A. J. Lovinger, Science **220**, 1115 (1983).
[3] G. I. Taylor, Proc. R. Soc. London, Ser. A **A146**, 501 (1934).
[4] B. J. Bentley and L. G. Leal, J. Fluid Mech. **167**, 219 (1986).
[5] J. J. L. Higdon, Phys. Fluids A **5**, 274 (1993).
[6] D. P. Pope and A. Keller, Colloid Polym. Sci. **255**, 633 (1977).
[7] S. Torza, J. Polym. Sci., Polym. Phys. Ed. **13**, 43 (1975).
[8] B. J. Bentley and L. G. Leal, J. Fluid Mech. **167**, 241 (1986).
[9] Y. T. Hu and A. Lips, Phys. Rev. Lett. **91**, 044501 (2003).
[10] H. Yang, C. C. Park, Y. T. Hu, and L. G. Leal, Phys. Fluids **13**, 1087 (2001).
[11] C. L. Colyer, T. Tang, N. Chiem, and D. J. Harrison, Electrophoresis **18**, 1733. (1997).
[12] D. R. Reyes, D. Iossifidis, P. A. Auroux, and A. Manz, Anal. Chem. **74**, 2623 (2002).
[13] J. Knight, Nature (London) **418**, 474 (2002).
[14] J S. Hur, E. S. G. Shaqfeh, H. P. Babcock, and S. Chu, Phys. Rev. E **66**, 011915 (2002).
[15] C. M. Schroeder, H. P. Babcock, E. S. G. Shaqfeh, and S. Chu, Science **301**, 1515 (2003).
[16] G. Astarita, J. Non-Newtonian Fluid Mech. **6**, 69 (1979).
[17] J P. Shelby, D. S. W. Lim, J. S. Kuo, and D. T. Chiu, Nature (London) **425**, 38 (2003).
[18] See EPAPS Document No. E-APPLAB-84-047426 for flow visualization videos and additional simulation results. A direct link to this document may be found in the online article's HTML reference section. The document may also be reached via the EPAPS homepage (http://www.aip.org/pubservs/epaps html) or from ftp.aip.org in the directory /epaps/. See the EPAPS homepage for more information.
[19] Although simple shear may also be obtained using rollers [in the small gap limit between two rollers, or between parallel belt drives (Ref. 3)], simple shear cannot be obtained in the four-roll mill, because its square geometric arrangement does not correspond to the small gap limit.
[20] A. Groisman, M. Enzelberger, and S. R. Quake, Science **300**, 955 (2003).
[21] http://www.pdesolutions.com. Certain commercial materials and equipment are identified in this paper in order to adequately specify the experimental procedure. In no case does such identification imply recommendation or endorsement by the National Institute of Standards and Technology, nor does it imply that these are necessarily the best available for the purpose.